Confined Ionic Liquid in an Ionic Porous Aromatic Framework for Gas Separation

Ziqi Tian,[†,‡] Sheng Dai,[§,∥] and De-en Jiang*[,‡]

[†]Ningbo Institute of Materials Technology & Engineering, Chinese Academy of Sciences, 1219 Zhongguan West Road, Zhenhai District, Ningbo 315201, P.R. China
[‡]Department of Chemistry, University of California, Riverside, California 92521, United States
[§]Department of Chemistry, University of Tennessee, Knoxville, Tennessee 37996, United States
[∥]Chemical Sciences Division, Oak Ridge National Laboratory, Oak Ridge, Tennessee 37831, United States

Abstract:

Ionic liquids (ILs) and porous frameworks are commonly employed in gas separation, but rarely together. To leverage their combined advantages, we designed a novel system comprising an ionic liquid inside a charged porous-polymer framework. A positively charged ionic porous aromatic framework was impregnated with an ionic liquid to confine the cations and anions inside the polymeric framework via electrostatic interactions. Molecular dynamics and free energy simulations were performed to determine the solubility, diffusivity, and hence permeability of CO_2 and CH_4 through the composite material. We found that the polymeric framework introduces nanoscale space in the confined IL, improving gas solubility, while the IL promotes gas transport in the porous structure. The confinement impacts CO_2 and CH_4 very differently regarding their solubility and diffusivity. Through tuning of the ionic-liquid loading, both high CO_2 permeability and high CO_2/CH_4 selectivity could be achieved, overcoming the Robeson upper bound. This work highlights the advantages of confined ionic liquids in an ionic porous-polymer framework in enhancing selective gas separation.

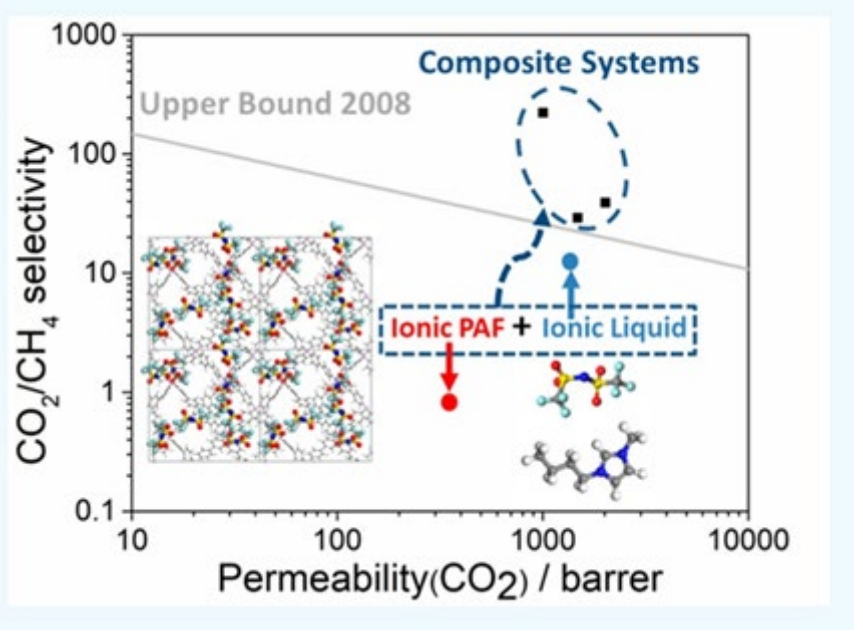

Keywords:

ionic liquids, porous polymers, molecular dynamics, gas separations, membranes, confinement

Acknowledgements:

This work was sponsored by the U.S. Department of Energy, Office of Science, Office of Basic Energy Sciences, Chemical Sciences, Geosciences, and Biosciences Division. This research used resources of the National Energy Research Scientific Computing Center, a DOE Office of Science User Facility sup- ported by the Office of Science of the U.S. Department of Energy under Contract DE-AC02-05CH11231.

Introduction

Efficient gas separations are essential to the chemical industry and environmental remediation. Membrane-based technology has become particularly appealing due to their energy efficiency and small footprint.[1–3] Traditional membrane separation via polymers is governed by the solution-diffusion mechanism, leading to a trade-off between permeability and selectivity called the Robeson upper bound.[4,5] Materials with specific affinity to a permeate molecule and uniform nanoscale pores are supposed to circumvent the limit.[6,7]

Ionic liquids (ILs) are widely used in a supported liquid membrane for gas separation.[8,9] They boast of negligible vapor pressure, good chemical and thermal stabilities, and great chemical tunability for gas separations.[10,11] But their liquid nature limits the membrane applications to low pressures. In addition, many ILs have high viscosity.

Porous materials such as metal organic frameworks (MOFs)[12–15] and covalent organic frameworks (COFs)[16,17] are popular sorbents for gas separations. Porous aromatic frameworks (PAFs) as a porous organic polymer also attracted great interest.[18] These materials possess large free volume and relatively uniform pore size ranging from several angstroms to a few nanometers. Recently, much effort has been devoted to developing membranes for these porous materials. For instance, incorporating MOF-based nanostructures into polymeric matrixes endowed composite membranes with outstanding gas separation performance.[19-21] COF and MOF membranes could also grow on a porous substrate via surface fabrication.[22,23] By controlling the thickness and component of the coating layer, gas separation would be significantly improved. Further, nanosheets with suitable aperture were exfoliated from bulk layered MOFs that could separate gas molecules by molecular sieving.[24,25]

Combining ILs and porous materials can lead to new avenues for discovering separation media. For example, a recent computational proof-of-concept demonstrated ion-gated gas separation through an IL/porous-graphene composite membrane where the ions of the IL are confined on a two-dimensional surface.26 Three-dimensional porous frameworks can offer even more flexibility in confining the ions and tune the pore size and the interaction for gas selectivity.27 Some MOF-IL composites have been designed theoretically[28–32] and synthesized experimentally[33–37] for membrane gas separation. For example, Yang et al. prepared IL/ZIF-8 composites that have high CO_2/CH_4 selectivity and CO_2 permeability.[33] A more recent study showed that the IL/ZIF-8 core−shell composite can dramatically increase CO_2/CH_4 adsorption selectivity.[38]

A critical concern in preparing the composite of a fluid and a nanoporous solid is how to disperse the liquid evenly in the pores of the framework. To this end, interaction between the IL and the porous framework has to be strengthened as much as possible. Given the ionic nature of the IL, one obvious idea would be to use an ionic porous framework to maximize the electrostatic interaction with the confined IL. Recently, a series of ionic covalent frameworks was reported,[39–43] which provide an ideal microenvironment to confine an IL for gas separations.

A typical such ionic covalent framework is quaternary-phosphonium-functionalized ionic porous aromatic framework (iPAF). Hence, an IL confined in an ionic porous polymer such as iPAF would provide an ideal system to understand how the confined ions in a 3D framework modulate gas separation. To this end, herein we used the iPAF as the porous framework to build up the IL-iPAF composite systems and simulate their performance for CO_2/CH_4 membrane separation in an effort to shed light on how the gas solubility and diffusivity are affected and can be tuned in the composite systems.

Simulation Models and Methods

Using phosphorous atoms to replace the sp^3-C nodes in the ideal diamond-like PAF-1 structure (Figure 1a),[44] the iPAF structure can be obtained (Figure 1b). The positive charges on the P atoms are balanced by the counter anions (green balls in Figure 1b). Structure and cell size of the iPAF with the TFSI anion were

optimized with density functional theory (DFT) using Vienna *ab initio* simulation package (VASP).[45] The Perdew−Burke−Erzerhof (PBE) functional[46] was employed with projector-augmented wave method (PAW)[47] to describe the electronic structure. Energy cutoff for the planewaves was set to be 400 eV, and only the Γ-point was used to sample the Brillouin zone. Because in the iPAF and IL-iPAF systems the electrostatic interaction dominates over the van der Waals interaction, we did not include dispersion in our DFT geometry optimizations.

A commonly studied IL, [bmim][TFSI] (Figure 1c), was chosen to fill into the porous structure of the iPAF-TFSI system. We examined various IL uptakes, from 0 to 18 ion pairs per unit cell. Molecular dynamics (MD) simulations were carried out on the 2 × 2 × 2 supercell model with Lammps under the NPT ensemble.[48] We used the FFtool code to assist in generating parameter files of the OPLS-AA type.[49] All the force field parameters are provided in the Supporting Information. Atomic charges were scaled by 0.8 to consider polarization and charge transfer, also in accordance with fitted charges of framework. EPM2 models were used to simulate gases.[50] The electrostatic interaction was summed with the PPPM method. The cutoff for non- bonded interactions was 12 Å, and long-range corrections were applied. Simulated systems were heated to 800 K for 10 ns and quenched to 300 K in 10 ns. Subsequently equilibrium MD simulations were run at 300 K for 25 ns. Nose−Hoover thermostat was employed to control temperature with a damping constant of 100 ps, while the Nose− Hoover barostat was used to maintain pressure at 1 atm with a damping constant of 500 ps. For comparison, the bulk IL was simulated with the same force-field and control parameters for a cubic-box supercell containing 100 ion pairs.

Gas diffusivity (D) in the composite system was obtained from the slope of the mean squared displacement (MSD) in the MD trajectory. To avoid random error, 20 paralleled 25 ns-MD simulations were performed for each system. Previous simulations indicated that the gas loading had little influence on MSD,[51−53] so we placed 10 gas mole- cules in each simulation box. Next, free energy perturbation (FEP) approach was implemented to compute gas solvation free energy,[54] ΔG_{sol}, and then to estimate solubility (S):

$$S = \frac{1}{RT}\exp\left(-\frac{\Delta G_{sol}}{RT}\right) \qquad (1)$$

The soft-core potential for gas was used to avoid singularity issues. Coupling parameter λ varied from both 0 to 1 and 1 to 0 at an interval of 0.0025, so 400 intermediate states in total; for each λ value or state, 100 ps of simulation was run for a total simulation time of 40 ns. Multiple independent runs were carried out to obtain average ΔG_{sol}.

To validate parameters and the method, we first computed the permeability ($P = D \times S$) and selectivity in bulk [bmim][TFSI]. Some important properties, such as the Henry's Law constant (H) and gas permeability, have been measured experimentally.[33,55] We compared the simulated values with available experimental data in Table 1. One can see that our simulations reproduce permeability and selectivity in good agreement with experiment. We further applied this approach to predict the gas separation performance in [bmim][TFSI]/ZIF-8 and found that the predicted CO_2/CH_4 sele vity (40.5) is in good agreement with the experiment (30 ∼ 40).[33]

Results and Discussion

Structure of iPAF-TFSI. We started with the diamond-like structure for iPAF-TFSI (Figure 2a) with a lattice parameter of 24.2 Å based on the parent PAF-1 structure (Figure 1a). Then, we allowed the lattice parameters to change and obtained a new distorted iPAF-TFSI structure with a much smaller lattice parameter of 17.8 Å (Figure 2b). Both the force-field-based and DFT-based calculations found the distorted structure energetically more favorable than the diamond-like structure, by 4.40 and 2.36 eV/cell, respectively. The optimized, distorted structure has a much smaller free volume. Previous experimental studies also indicated more condensed networks for some PAF derivatives than the ideal diamond

topology.[56] The iPAF− IL composites examined below will be therefore based on the more stable, distorted structure of iPAF-TFSI and the popular IL, [bmim][TFSI] (Figure 1c).

Structure and Properties of the iPAF−[bmim][TFSI] Composite. We next simulated the composite system with various uptakes of the [bmim][TFSI] IL. Because the parent iPAF has a cubic initial structure and we used a large cell of many ion pairs inside the iPAF, we assumed that the IL-iPAF systems would be in general isotropic. So, in our NPT simu- lations, we maintained the cubic cell shape but allowed only the cell size or volume to vary. We think that this is a good approximation to generate reproducible and consistent gas solubility and diffusivity data inside the IL-iPAF systems. For simplicity, the composite containing n IL pairs per unit cell is labeled as iPAF-nIL. Figure 3 shows the structures of the iPAF-nIL systems for n = 4, 8, 12, and 16, corresponding to [bmim]/P molar ratios of 0.5, 1.0, 1.5, and 2.0, respectively. One can see the gradually increasing lattice parameter, as more IL ion pairs are loaded into the iPAF, similar to the swelling behavior of a polymer. We found that as many as 16 IL pairs can be fully loaded into the iPAF framework. For modeling of gas permeation, we considered three composite systems with relatively high IL loadings, i.e., iPAF−8IL, iPAF−12IL, and iPAF− 16IL.

Radial distributions functions (RDFs) of ions to the phosphorous node in the composites are plotted in Figure 4. The smooth and broad RDF curves of ions indicate the fluid nature of the IL in the confined environment. Because the positive charges of the iPAF framework are mainly centered on the P atoms, so they attract the $[TFSI]^-$ anions and repel the $[bmim]^+$ cations, and the RDFs in Figure 4 show that the $[TFSI]^-$ anions (dashed lines) are closer than the $[bmim]^+$ cations (solid lines) are to the P atoms in iPAF. Compared to the peaks of the $[TFSI]^-$ anions (∼7.0 Å), the distributions of the $[bmim]^+$ cations are broader (8−10 Å) and shift to the right with the IL loading, indicating a weakened interaction between the cations and the iPAF with the IL loading.

MSDs of ions are plotted in Figure 5. One can see that the $[TFSI]^-$ anions are rather immobile in the iPAF-TFSI framework itself, due to the strong attraction by the positively charged framework. As shown in Figure S1, the MSDs of cation and anion in iPAF-4IL are quite similar to the MSD of anion in iPAF-TFSI; in other words, the ions are tightly trap- ped in the pores when the loading is low. On the other hand, both cations and anions are mobile in the iPAF−IL composites with higher IL loadings at the simulation temperature (300 K), even though they move much slower than ions in the bulk ionic liquid (Figure 5). Because anions are more strongly attracted to the positively charged framework, the $[TFSI]^-$ anions move much slower than the $[bmim]^+$ cations in the same composite. Interestingly, the anion MSDs are almost identical in the three composites of different IL loadings, but the MSD of the cation increases with the loading of the ionic liquid. From iPAF−8IL to iPAF−16IL, the cation diffusivity increases from 0.0787 to 0.121 $Å^2$/ns. The increasing cation diffusivity correlates with both the lattice expansion (Figure 3) and the weakened cation−framework interaction (Figure 4) with the IL loading. The higher mobility of the cations can help the transport of the gas molecules through the iPAF−IL composite.

Structure of CO_2 and CH_4 in the iPAF−[bmim][TFSI] Composite. To examine the performance of the iPAF−IL composite for CO_2/CH_4 separation, we first investigated the structure of CO_2 and CH_4 in the composites of different IL loadings. Figure 6 shows that the RDFs of CO_2 and CH_4 around the phosphorous nodes of the iPAF are almost the same at various loadings: the average positions of the first peaks for CO_2 and CH_4 are at 5.78 and 5.62 Å, respectively. Figure 7 plots the RDFs of gases around cations and anions. CO_2 has some closer contact with the anions than with the cations, while CH_4 has more probability around the anions than around the cations. Typical snapshots of gas molecules in the iPAF−12IL composite system are shown in Figure 8.

Performance of the iPAF−[bmim][TFSI] Composite for CO_2/CH_4 Separation. To estimate the gas permeability of the iPAF−[bmim][TFSI] composite membrane, we first sim- ulated the solvation free energy (ΔG_{sol}) and solubility (S) of CO_2 and CH_4 separation in the iPAF−[bmim][TFSI] composites of different IL loadings. Table 2 lists all simulated ΔG_{sol} of CO_2 and CH_4 in the iPAF−[bmim][TFSI] composites of various IL loadings. We then converted ΔG_{sol} to gas solubility at 298 K and 1 bar (Table 3). One can see that both

CO_2 and CH_4 solubilities are higher in the composite than in the bulk IL, while CH_4 solubility is much lower in the com- posite than in the iPAF itself, leading to a much higher solubility selectivity (SS) of CO_2/CH_4 in the composite than in the iPAF (Table 3). Interestingly, the iPAF−8IL composite's CO_2/CH_4 solubility selectivity is even higher than that of the bulk IL.

Table 3 further compares diffusivity (D) and permeability ($P = D \times S$) of CO_2 and CH_4 in the iPAF−[bmim][TFSI] composites as well as the selectivity. In the iPAF itself, CO_2 is adsorbed strongly inside the sorbent, leading to a low gas diffusivity. With the IL loading, the gas diffusivity increases, and there exists an optimal loading of iPAF−12IL. Although gas diffusivity is still lower than that in the bulk IL, the CO_2/CH_4 diffusivity selectivity (DS) is actually higher in the iPAF−IL composite than that in the bulk IL because the confined ions slow down CH_4 more than they do CO_2. The combined effect of solubility and diffusivity is a higher permeability of CO_2 and a higher CO_2/CH_4 permselectivity (PS) in the compos- ite than in either the bulk IL or the iPAF itself. We plot CO_2 permeability versus CO_2/CH_4 selectivity in Figure 9, together with the 2008 Robeson upper bound.[4] The simulated data for the bulk IL are in good agreement with the experiment. Compared with the bulk IL and the iPAF, all three composite systems show improved separation performances above the upper bound from our simulations. Especially, the iPAF−8IL system is most promising because at this loading both the solubility selectivity and the diffusivity selectivity are the highest (Table 3).

Implications of Our Simulation Results. Our simulation results in Table 3 and Figure 9 suggest a promising way to overcome the Robeson upper bound by using the iPAF/IL com- posite. Loading can be used as a parameter to further tune the performance. Recent experiments have demonstrated the advan- tages in combining MOFs and ILs for gas separation.[33,38,57] Here, we further show that a charged porous organic framework loaded with ILs holds the potential for breakthrough mem- brane performances. We think that this idea can also be applied to the porous organic polymers that do not necessarily have a well-defined periodic structure.

Conclusion

In summary, we designed and simulated a composite material made of an ionic liquid confined inside an ionic porous-polymer aromatic framework (iPAF−IL) for membrane gas separation of CO_2 and CH_4. We optimized the structure with density functional theory and performed classical molecular dynamics and free-energy simulations to determine the solubility, diffusivity, and hence permeability of CO_2 and CH_4 in the composite material of different IL loadings. We found that gas solubility is higher in the composite than in the bulk IL, more so for CO_2 than for CH_4, while gas diffusivity is lower in the composite than in the bulk IL, and the confined ions slow down CO_2 less than they do CH_4. As a result, both higher CO_2 permeability and higher CO_2/CH_4 selectivity were achieved in the composite than in the bulk IL or the iPAF itself. For certain loading, the simulated performance is significantly above the Robeson upper bound. This work shows the promise of confined ionic liquids in porous organic polymers in improving membrane gas separation.

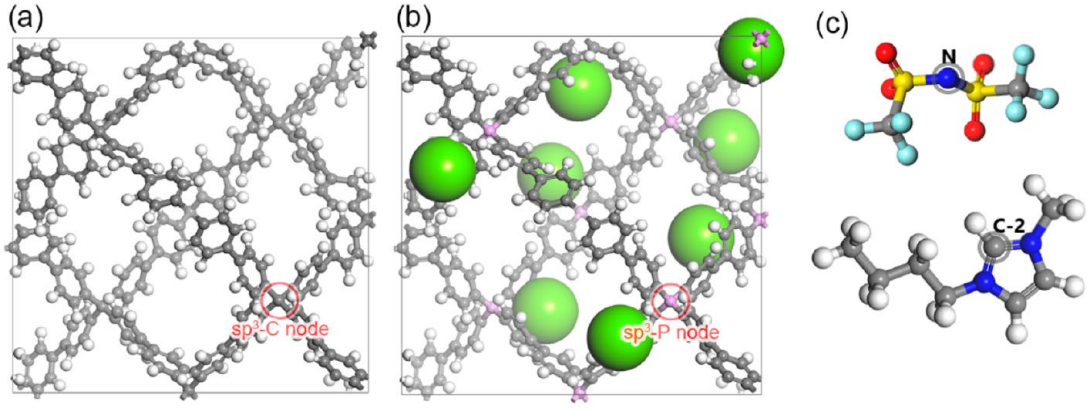

Figure 1. (a) Structure of the ideal diamond-like PAF-1: the bond between two sp^3-C atoms in the diamond structure is replaced by the biphenyl unit. (b) The structure of iPAF studied in this work: P atom nodes (pink) replace the sp^3-C nodes in PAF-1; each positively charged P node is balanced by an anion (large green ball). (c) Structures of [TFSI] anion and [bmim] cation: the N atom in the anion and the C-2 atom in the cation are marked for radial distribution function analysis later. Color code: white, H; grey, C; blue, N; red, O; cyan, F; yellow, S; pink, P.

Table 1. Comparison of Simulated and Experimental Henry's Law Constant (H), Diffusivity (D), Permeability (P), and Selectivity (S) of CO_2 and CH_4 in [bmim][TFSI]

	H_{CO_2} (MPa)	D_{CO_2} (Å^2/ns)	H_{CH_4} (MPa)	D_{CH_4} (Å^2/ns)	P_{CO_2} (barrer)	P_{CH_4} (barrer)	$S_{CO2/CH4}$
exptl[a]	3.5	58	52.4		1344	110	12.2
simulated	3.40	27.8	66.5	22.6	833	34.6	24.1

[a]Ref 55.

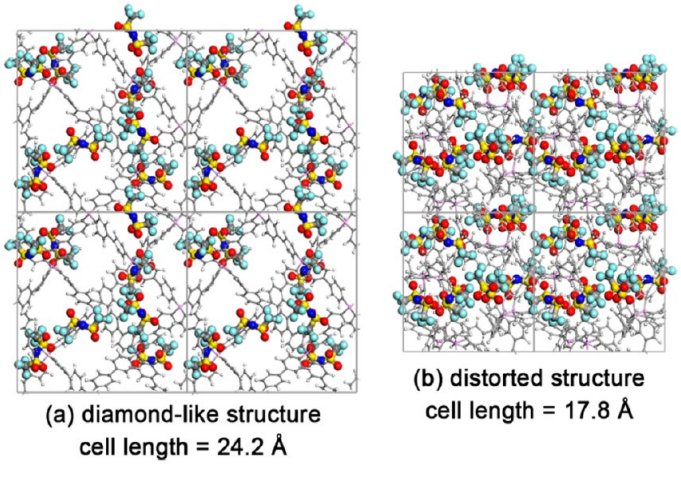

Figure 2. (a) The initial diamond-like iPAF-TFSI structure. (b) The distorted and shrunken structure after DFT geometry optimization. The structures are shown in a front view of a 2 × 2 × 2 supercell, with the unit cell length given; the iPAF framework in the line model, the TFSI anions in the CPK model. The color code is the same as that in Figure 1.

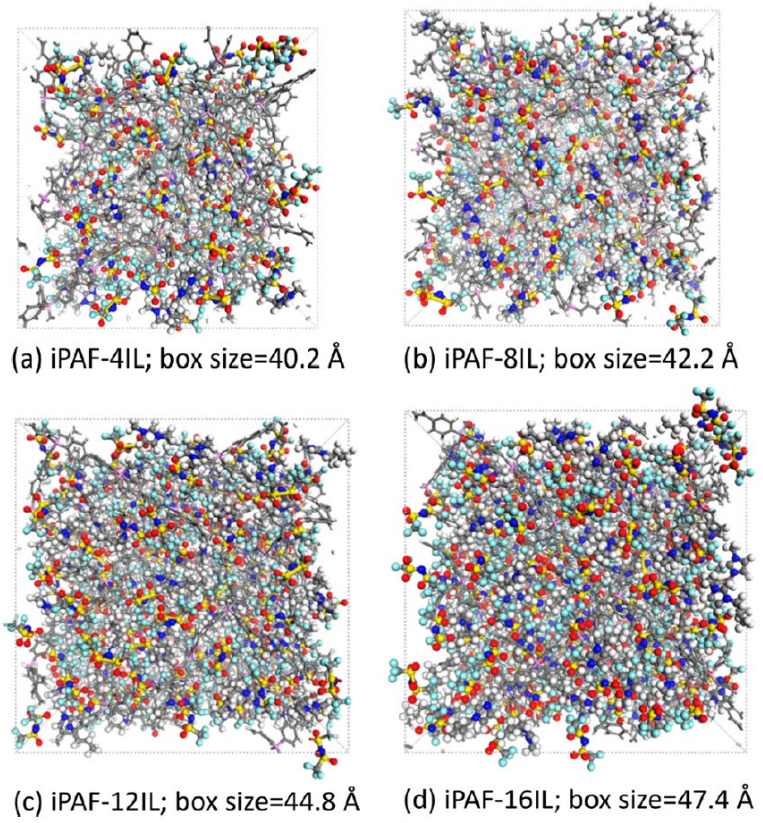

Figure 3. Snapshots of the iPAF-*n*IL composite systems: (a) $n = 4$; (b) $n = 8$; (c) $n = 12$; (d) $n = 16$. The corresponding IL/iPAF weight ratios are 0.625, 1.25, 1.875, and 2.50, respectively; the corresponding [bmim]/P molar ratios are 0.5, 1.0, 1.5, and 2.0, respectively.

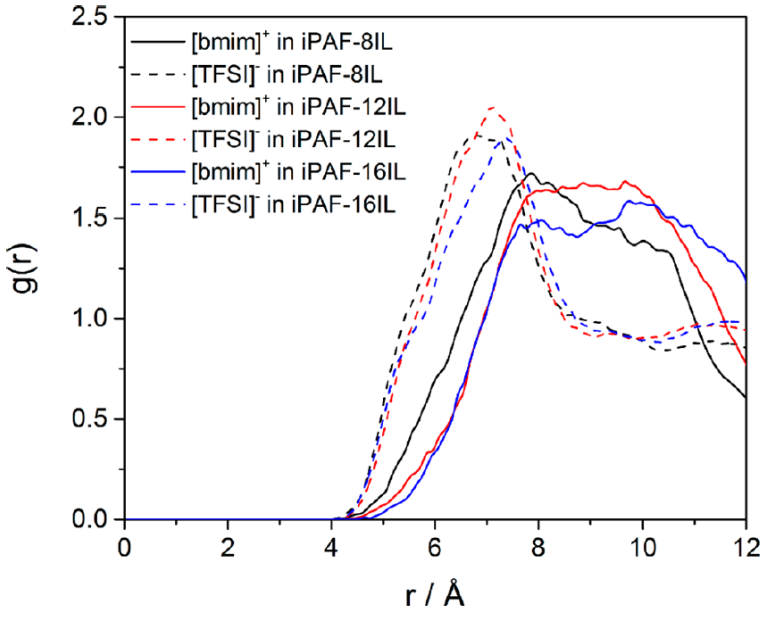

Figure 4. RDFs of $[bmim]^+$ cations (from the C-2 position on the imidazolium ring; Figure 1c) and $[TFSI]^-$ anions (from the N atom; Figure 1c) around the phosphorous node in the positively charged iPAF framework for iPAF−IL composites of different IL loadings.

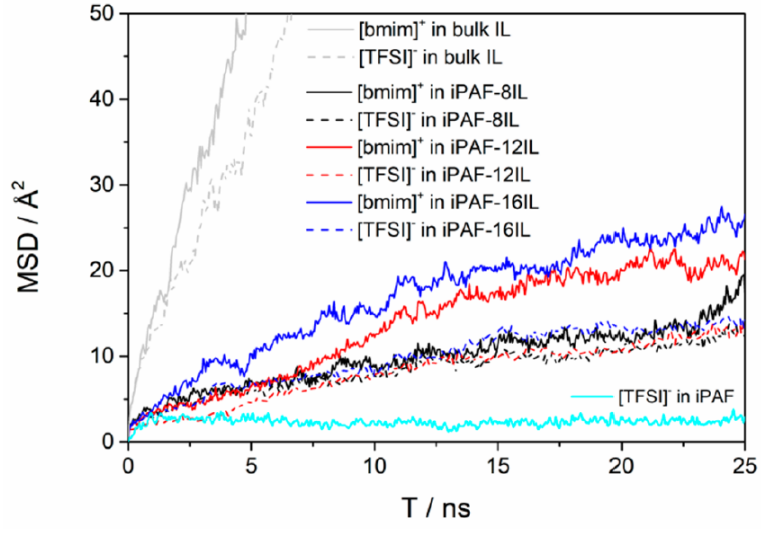

Figure 5. MSDs of cations and anions in the iPAF−[bmim][TFSI] composites of various IL loadings. For comparison, MSDs in the bulk IL and iPAF are also shown.

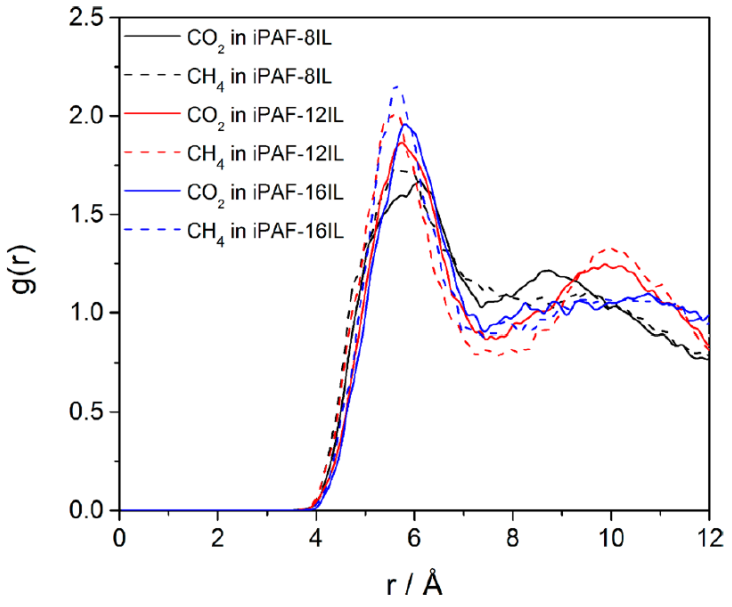

Figure 6. RDFs of gases (from the carbon atom) to the positively charged P nodes of iPAF.

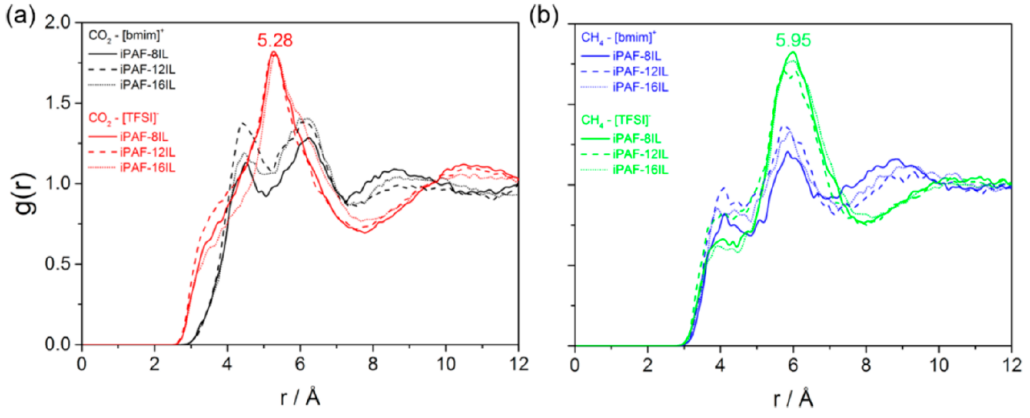

Figure 7. RDFs of (a) CO_2 and (b) CH_4 to the cations (represented by the C-2 position on the imidazolium ring) and anions (represented by the N atom) in composites with various IL loadings.

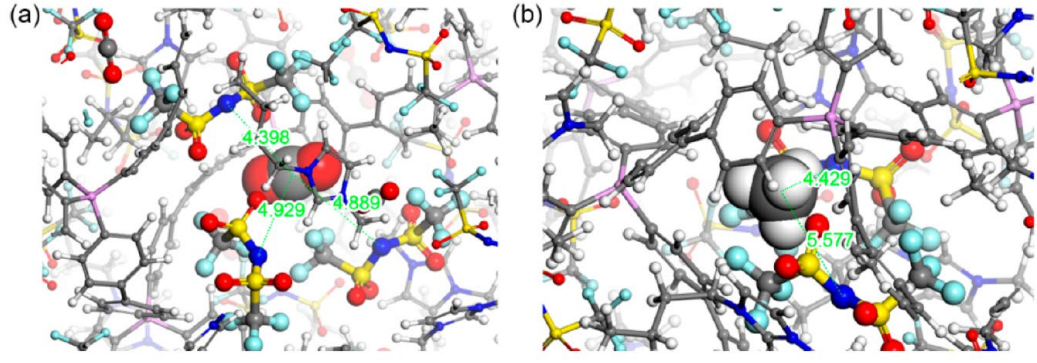

Figure 8. Typical snapshots of (a) CO_2 and (b) CH_4 molecules inside the iPAF−12IL composite.

Table 3. Simulated Solubility (S), Diffusivity (D), and Permeability (P) of CO_2 and CH_4 and Their Respective CO_2/CH_4 Selectivities (SS, DS, and PS) in the iPAF–[bmim][TFSI] Composites of Various IL Loadings[a]

	S_{CO_2} (mol/L^{-1}bar^{-1})	S_{CH_4} (mol/L^{-1}bar^{-1})	SS	D_{CO_2} (Å^2/ns)	D_{CH_4} (Å^2/ns)	DS	P_{CO_2} (barrer)	P_{CH_4} (barrer)	PS
bulk IL	0.102 (0.013)	0.0041 (0.0004)	24.9 (4.2)	27.8 (0.10)	22.6 (0.08)	1.23 (0.01)	834 (112)	34.6 (2.9)	24.1 (3.8)
iPAF–16IL	0.351 (0.112)	0.022 (0.002)	16.0 (6.3)	14.3 (0.09)	7.83 (0.04)	1.83 (0.02)	1479 (482)	50.9 (3.6)	29.1 (9.7)
iPAF–12IL	0.393 (0.025)	0.018 (0.005)	21.8 (6.9)	17.4 (0.05)	9.49 (0.04)	1.83 (0.01)	2018 (132)	51.7 (13.6)	39.0 (10.6)
iPAF–8IL	0.466 (0.174)	0.009 (0.001)	51.8 (22.3)	7.30 (0.04)	1.67 (0.08)	4.37 (0.23)	1002 (384)	4.5 (0.35)	223 (86.9)
iPAF	0.704 (0.173)	0.187 (0.055)	3.76 (2.07)	1.71 (0.02)	8.01 (0.03)	0.21 (0.003)	352 (96)	439 (89)	0.80 (0.31)

[a]For comparison, values in the bulk IL and the iPAF itself are also shown. Uncertainties (±) are given in parentheses. (SS=Solubility Selectivity, DS=Diffusion Selectivity, and PS=Permselectivity).

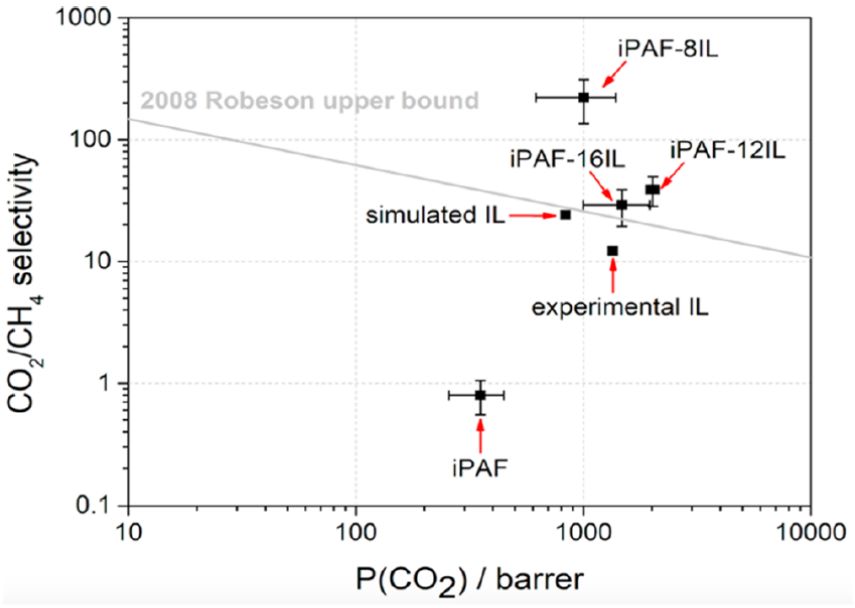

Figure 9. CO_2 permeability versus CO_2/CH_4 selectivity of composite with various ionic liquid loading.

References

(1) Baker, R. W. Future Directions of Membrane Gas Separation Technology. Ind. Eng. Chem. Res. 2002, 41, 1393−1411.
(2) Bernardo, P.; Drioli, E.; Golemme, G. Membrane Gas Separation: A Review/State of the Art. Ind. Eng. Chem. Res. 2009, 48, 4638−4663.
(3) Li, C.; Meckler, S. M.; Smith, Z. P.; Bachman, J. E.; Maserati, L.; Long, J. R.; Helms, B. A. Engineered Transport in Microporous Materials and Membranes for Clean Energy Technologies. Adv. Mater. 2018, 30, 1704953.
(4) Castro-Dominguez, B.; Leelachaikul, P.; Messaoud, S. B.; Takagaki, A.; Sugawara, T.; Kikuchi, R.; Oyama, S. T. The Optimal Point within the Robeson Upper Boundary. Chem. Eng. Res. Des. 2015, 97, 109−119.
(5) Robeson, L. M. The Upper Bound Revisited. J. Membr. Sci. 2008, 320, 390−400.
(6) Wang, J.; Zhu, J. Y.; Zhang, Y. T.; Liu, J. D.; Van der Bruggen, B. Nanoscale Tailor-Made Membranes for Precise and Rapid Molecular Sieve Separation. Nanoscale 2017, 9, 2942−2957.
(7) Wang, L.; Boutilier, M. S. H.; Kidambi, P. R.; Jang, D.; Hadjiconstantinou, N. G.; Karnik, R. Fundamental Transport Mechanisms, Fabrication and Potential Applications of Nanoporous Atomically Thin Membranes. Nat. Nanotechnol. 2017, 12, 509−522.
(8) Lozano, L. J.; Godínez, C.; de los Ríos, A. P.; Hernańdez- Fernańdez, F. J.; Sańchez-Segado, S.; Alguacil, F. J. Recent Advances in Supported Ionic Liquid Membrane Technology. J. Membr. Sci. 2011, 376, 1−14.
(9) Shang, D. W.; Liu, X. Y.; Bai, L.; Zeng, S. J.; Xu, Q. X.; Gao, H. S.; Zhang, X. P. Ionic Liquids in Gas Separation Processing. Curr. Opin. Green Sustain. Chem. 2017, 5, 74−81.
(10) Tome, L. C.; Marrucho, I. M. Ionic Liquid-Based Materials: A Platform to Design Engineered CO_2 Separation Membranes. Chem. Soc. Rev. 2016, 45, 2785−2824.
(11) Zeng, S.; Zhang, X.; Bai, L.; Zhang, X.; Wang, H.; Wang, J.; Bao, D.; Li, M.; Liu, X.; Zhang, S. Ionic Liquid-Based CO_2 Capture Systems: Structure, Interaction and Process. Chem. Rev. 2017, 117, 9625−9673.
(12) Denny, M. S.; Moreton, J. C.; Benz, L.; Cohen, S. M. Metal- Organic Frameworks for Membrane-Based Separations. Nat. Rev. Mater. 2016, 1, 17.
(13) Duan, J. G.; Jin, W. Q.; Kitagawa, S. Water-Resistant Porous Coordination Polymers for Gas Separation. Coord. Chem. Rev. 2017, 332, 48−74.
(14) Yu, J.; Xie, L. H.; Li, J. R.; Ma, Y.; Seminario, J. M.; Balbuena,P. B. CO_2 Capture and Separations Using MOFs: Computational and Experimental Studies. Chem. Rev. 2017, 117, 9674−9754.
(15) Zhao, X.; Wang, Y.; Li, D. S.; Bu, X.; Feng, P. Metal-Organic Frameworks for Separation. Adv. Mater. 2018, 30, 1705189.
(16) Diaz, U.; Corma, A. Ordered Covalent Organic Frameworks, COFs and PAFs. From Preparation to Application. Coord. Chem. Rev. 2016, 311, 85−124.
(17) Zang, Y.; Aoki, T.; Teraguchi, M.; Kaneko, T.; Ma, L. Q.; Jia, H. G. Two-Dimensional and Related Polymers: Concepts, Synthesis, and their Potential Application as Separation Membrane Materials. Polym. Rev. 2015, 55, 57−89.
(18) Pei, C.; Ben, T.; Qiu, S. Great Prospects for PAF-1 and its Derivatives. Mater. Horiz. 2015, 2, 11−21.
(19) Kertik, A.; Wee, L. H.; Pfannmöller, M.; Bals, S.; Martens, J. A.; Vankelecom, I. F. J. Highly Selective Gas Separation Membrane Using in situ Amorphised Metal−Organic Frameworks. Energy Environ. Sci. 2017, 10, 2342−2351.
(20) Kong, C.; Du, H.; Chen, L.; Chen, B. Nanoscale MOF/ Organosilica Membranes on Tubular Ceramic Substrates for Highly Selective Gas Separation. Energy Environ. Sci. 2017, 10, 1812−1819.
(21) Rodenas, T.; Luz, I.; Prieto, G.; Seoane, B.; Miro, H.; Corma, A.; Kapteijn, F.; Llabres, I. X. F. X.; Gascon, J. Metal-Organic Framework Nanosheets in Polymer Composite Materials for Gas Separation. Nat. Mater. 2015, 14, 48−55.
(22) Lu, H.; Wang, C.; Chen, J.; Ge, R.; Leng, W.; Dong, B.; Huang, J.; Gao, Y. A Novel 3d Covalent Organic Framework Membrane Grown on a Porous alpha-Al_2O_3 Substrate under Solvothermal

Conditions. Chem. Commun. 2015, 51, 15562−15565.
(23) Li, W.; Su, P.; Li, Z.; Xu, Z.; Wang, F.; Ou, H.; Zhang, J.; Zhang, G.; Zeng, E. Ultrathin Metal-Organic Framework Membrane Production by Gel-Vapour Deposition. Nat. Commun. 2017, 8, 406.
(24) Peng, Y.; Li, Y. S.; Ban, Y. J.; Jin, H.; Jiao, W. M.; Liu, X. L.; Yang, W. S. Metal-Organic Framework Nanosheets as Building Blocks for Molecular Sieving Membranes. Science 2014, 346, 1356− 1359.
(25) Peng, Y.; Li, Y.; Ban, Y.; Yang, W. Two-Dimensional Metal- Organic Framework Nanosheets for Membrane-Based Gas Separa- tion. Angew. Chem., Int. Ed. 2017, 56, 9757−9761.
(26) Tian, Z. Q.; Mahurin, S. M.; Dai, S.; Jiang, D. E. Ion-Gated Gas Separation through Porous Graphene. Nano Lett. 2017, 17, 1802− 1807.
(27) Zhang, S.; Zhang, J.; Zhang, Y.; Deng, Y. Nanoconfined Ionic Liquids. Chem. Rev. 2017, 117, 6755−6833.
(28) Li, Z. J.; Xiao, Y. L.; Xue, W. J.; Yang, Q. Y.; Zhong, C. L. Ionic Liquid/Metal-Organic Framework Composites for H_2S Removal from Natural Gas: A Computational Exploration. J. Phys. Chem. C 2015, 119, 3674−3683.
(29) Chen, Y.; Hu, Z.; Gupta, K. M.; Jiang, J. Ionic Liquid/Metal−Organic Framework Composite for CO_2 Capture: A Computational Investigation. J. Phys. Chem. C 2011, 115, 21736−21742.
(30) Gupta, K. M.; Chen, Y.; Hu, Z.; Jiang, J. Metal-Organic Framework Supported Ionic Liquid Membranes for CO_2 Capture: Anion Effects. Phys. Chem. Chem. Phys. 2012, 14, 5785−94.
(31) Shi, W.; Luebke, D. R. Enhanced Gas Absorption in the Ionic Liquid 1-N-Hexyl-3-Methylimidazolium Bis(Trifluoromethylsulfonyl)- Amide ([Hmim][Tf_2N]) Confined in Silica Slit Pores: A Molecular Simulation Study. Langmuir 2013, 29, 5563−5572.
(32) Mousavi-Khoshdel, M.; Targholi, E.; Momeni, M. J. First- Principles Calculation of Quantum Capacitance of Codoped Graphenes as Supercapacitor Electrodes. J. Phys. Chem. C 2015, 119, 26290−26295.
(33) Ban, Y.; Li, Z.; Li, Y.; Peng, Y.; Jin, H.; Jiao, W.; Guo, A.; Wang, P.; Yang, Q.; Zhong, C.; Yang, W. Confinement of Ionic Liquids in Nanocages: Tailoring the Molecular Sieving Properties of ZIF-8 for Membrane-Based CO_2 Capture. Angew. Chem., Int. Ed. 2015, 54, 15483−15487.
(34) Kinik, F. P.; Altintas, C.; Balci, V.; Koyuturk, B.; Uzun, A.; Keskin, S. [BMIM][PF_6] Incorporation Doubles CO_2 Selectivity of ZIF-8: Elucidation of Interactions and Their Consequences on Performance. ACS Appl. Mater. Interfaces 2016, 8, 30992
(35) Koyuturk, B.; Altintas, C.; Kinik, F. P.; Keskin, S.; Uzun, A. Improving Gas Separation Performance of ZIF-8 by [BMIM][BF_4] Incorporation: Interactions and Their Consequences on Performance. J. Phys. Chem. C 2017, 121, 10370−10381.
(36) Ma, J.; Ying, Y.; Guo, X.; Huang, H.; Liu, D.; Zhong, C. Fabrication of Mixed-Matrix Membrane Containing Metal−Organic Framework Composite with Task-Specific Ionic Liquid for Efficient CO_2 Separation. J. Mater. Chem. A 2016, 4, 7281−7288.
(37) Sezginel, K. B.; Keskin, S.; Uzun, A. Tuning the Gas Separation Performance of CuBTC by Ionic Liquid Incorporation. Langmuir 2016, 32, 1139−1147.
(38) Zeeshan, M.; Nozari, V.; Yagci, M. B.; Isık, T.; Unal, U.; Ortalan, V.; Keskin, S.; Uzun, A. Core−Shell Type Ionic Liquid/ Metal Organic Framework Composite: An Exceptionally High CO_2/ CH_4 Selectivity. J. Am. Chem. Soc. 2018, 140, 10113.
(39) Zhang, Q.; Zhang, S.; Li, S. Novel Functional Organic Network Containing Quaternary Phosphonium and Tertiary Phosphorus. Macromolecules 2012, 45, 2981−2988.
(40) Fischer, S.; Schimanowitz, A.; Dawson, R.; Senkovska, I.; Kaskel, S.; Thomas, A. Cationic Microporous Polymer Networks by Polymerisation of Weakly Coordinating Cations with CO_2-Storage Ability. J. Mater. Chem. A 2014, 2, 11825−11829.
(41) Yan, Z.; Yuan, Y.; Tian, Y.; Zhang, D.; Zhu, G. Highly Efficient Enrichment of Volatile Iodine by Charged Porous Aromatic Frameworks with Three Sorption Sites. Angew. Chem., Int. Ed. 2015, 54, 12733−12737.
(42) Sun, J. K.; Antonietti, M.; Yuan, J. Nanoporous Ionic Organic Networks: From Synthesis to Materials Applications. Chem. Soc. Rev. 2016, 45, 6627−6656.
(43) Roeser, J.; Prill, D.; Bojdys, M. J.; Fayon, P.; Trewin, A.; Fitch, A. N.; Schmidt, M. U.; Thomas,

A. Anionic Silicate Organic Frameworks Constructed from Hexacoordinate Silicon Centres. Nat. Chem. 2017, 9, 977−982.
(44) Ben, T.; Ren, H.; Ma, S.; Cao, D.; Lan, J.; Jing, X.; Wang, W.; Xu, J.; Deng, F.; Simmons, J. M.; Qiu, S.; Zhu, G. Targeted Synthesis of a Porous Aromatic Framework with High Stability and Exceptionally High Surface Area. Angew. Chem., Int. Ed. 2009, 48, 9457−9460.
(45) Kresse, G.; Furthmuller, J. Efficient Iterative Schemes for ab Initio Total-Energy Calculations Using a Plane-Wave Basis Set. Phys. Rev. B: Condens. Matter Mater. Phys. 1996, 54, 11169−11186.
(46) Perdew, J. P.; Burke, K.; Ernzerhof, M. Generalized Gradient Approximation Made Simple. Phys. Rev. Lett. 1996, 77, 3865−3868.
(47) Blochl, P. E. Projector Augmented-Wave Method. Phys. Rev. B: Condens. Matter Mater. Phys. 1994, 50, 17953−17979.
(48) Plimpton, S. Fast Parallel Algorithms for Short-Range Molecular-Dynamics. J. Comput. Phys. 1995, 117, 1−19.
(49) Padua, A. FFtool. https://github.com/agiliopadua/fftool (accessed Oct 15, 2017).
(50) Harris, J. G.; Yung, K. H. Carbon Dioxide's Liquid-Vapor Coexistence Curve And Critical Properties as Predicted by a Simple Molecular Model. J. Phys. Chem. 1995, 99, 12021−12024.
(51) Hansen, N.; Jakobtorweihen, S.; Keil, F. J. Reactive Monte Carlo and Grand-Canonical Monte Carlo Simulations of the Propene Metathesis Reaction System. J. Chem. Phys. 2005, 122, 164705.
(52) Dubbeldam, D.; Calero, S.; Ellis, D. E.; Snurr, R. Q. RASPA: Molecular Simulation Software for Adsorption and Diffusion in Flexible Nanoporous Materials. Mol. Simul. 2016, 42, 81−101.
(53) Liu, H.; Dai, S.; Jiang, D. E. Structure and Dynamics of CO_2 and N_2 in a Tetracyanoborate Based Ionic Liquid. Phys. Chem. Chem. Phys. 2014, 16, 1909−1913.
(54) Liu, H.; Dai, S.; Jiang, D.-e. Molecular Dynamics Simulation of Anion Effect on Solubility, Diffusivity, and Permeability of Carbon Dioxide in Ionic Liquids. Ind. Eng. Chem. Res. 2014, 53, 10485− 10490.
(55) Friedrich, M. F.; Kokolakis, S.; Lucas, M.; Claus, P. Measuring Diffusion and Solubility of Slightly Soluble Gases in [CnMIM][NTf_2] Ionic Liquids. J. Chem. Eng. Data 2016, 61, 1616
(56) Xiang, Z.; Mercado, R.; Huck, J. M.; Wang, H.; Guo, Z.; Wang, W.; Cao, D.; Haranczyk, M.; Smit, B. Systematic Tuning and Multifunctionalization of Covalent Organic Polymers for Enhanced Carbon Capture. J. Am. Chem. Soc. 2015, 137, 13301−13307.
(57) Kinik, F. P.; Uzun, A.; Keskin, S. Ionic Liquid/Metal−Organic Framework Composites: From Synthesis to Applications. ChemSu- sChem 2017, 10, 2842